THE ASTROPHYSICAL JOURNAL, 504:375–389, 1998 September 1

VLA OBSERVATIONS OF HYDROGEN AND CARBON RECOMBINATION LINES TOWARD W3A AT 1.4 GHz

NIMISHA G. KANTHARIA[1] AND K. R. ANANTHARAMAIAH[2]
Raman Research Institute, C. V. Raman Avenue, Bangalore 560 080, India

AND

W. M. GOSS
National Radio Astronomy Observatory, P. O. Box O, 1003 Lopezville Road, Socorro, NM 87801
Received 1997 December 8; accepted 1998 March 3

ABSTRACT

We present high-sensitivity, high-resolution VLA observations of the W3 complex of H II regions in the 168α recombination lines of hydrogen, carbon, and sulphur. The H 168α line from W3A consists of two components: a broad line (width $\sim$27 km s^{-1}) and a narrow line (width $\sim$7 km s^{-1}). The narrow hydrogen and carbon line emissions over W3A, although overlapping, are not entirely coextensive. The carbon line is possibly correlated with the molecular gas near W3A. Stimulated emission is the main mechanism for the narrow hydrogen line emission. The width of the H^0 line gives an upper limit of $\sim$1000 K for the electron temperature of the partially ionized gas. The electron density ranges from 10 to 80 cm^{-3} in the narrow hydrogen line region and from 10 to 60 cm^{-3} in the carbon-line region. We determined the electron temperature of the classical H II region W3A from the continuum brightness to be $\sim$9000 K. The rms n_e of this H II region is $\sim$2200 cm^{-3}, and the true n_e, determined from a pressure-broadened profile of the H 171η (8.6 GHz) line, is $\sim 2 \times 10^4$ cm^{-3}. Using these two values of electron densities, we determine a lower limit to the filling factor (0.01). Such a low value can be interpreted as an effect of density inhomogeneities in the medium.

Subject headings: H II regions — ISM: individual (W3A) — line: profiles — radio lines: ISM

1. INTRODUCTION

W3 (core) ($l = 133°$, $b = 1.2°$) is a complex of Galactic H II regions and molecular clouds at a distance of 2.3 kpc (Georgelin & Georgelin 1976) in the Perseus spiral arm. This source consists of H II regions in various evolutionary stages, with angular sizes ranging from less than 5″ to 50″. W3A is the largest and most evolved component, and it has been widely studied in continuum and spectral lines over a wide range of frequencies. Single-dish radio recombination line observations of W3A at centimeter wavelengths (e.g., Pankonin et al. 1977) show narrow ($\Delta V \sim$ 5–8 km s^{-1}) hydrogen, carbon, and sulphur lines in addition to the expected relatively broad ($\Delta V \sim$ 25 km s^{-1}) hydrogen and helium lines. The broad lines arise in the hot H II region; the narrow lines are believed to arise in a partially ionized medium adjacent to and possibly surrounding the H II region. The first interferometric observations of recombination lines from W3A were made by van Gorkom (1980), who found that the hydrogen line consisted of two components of widths $\sim$70 km s^{-1} and $\sim$7 km s^{-1}. The broad component detected in the interferometric observations was weak ($T_l/T_c = 0.002$) and almost 3 times as broad as the line observed in single-dish observations ($\sim$27 km s^{-1}). A broad hydrogen line ($\sim$70 km s^{-1}) was also detected in the interferometric observations of Roelfsema & Goss (1991). Thus, although the width of the narrow hydrogen component is strong and appears as a sharp feature above the broad pedestal, matched in the single-dish and interferometric observations, the width of the broad component appeared to be discrepant in the two different types of observation.

Most of the observations toward W3A have detected narrow radio recombination lines of carbon in addition to that of hydrogen, indicating the presence of an associated C II region. These lines could be explained if the emitting region has a temperature of $\sim$150 K and an electron density of $\sim$25 cm^{-3} (Pankonin et al. 1977). The major mechanism for the carbon line is stimulated emission from a region in front of the bright H II region. The carbon line emission from W3A near 1.4 GHz was imaged by Roelfsema, Goss, & Wilson (1987) with a resolution of $\sim$14″; the C II emission is confined to the location of the continuum source, thus confirming the importance of stimulated emission. However, the line emission displayed structure that is distinct from that of the continuum, and these authors interpret it as being an effect of variations in the physical properties of the emitting gas.

Although it appears that the narrow hydrogen and the narrow carbon lines arise in a relatively cooler partially ionized medium adjacent to the H II region, it is not clear whether the two lines arise from the same region. The spatial distributions of both the recombination lines should be similar if they arise in coexistent media. If the spatial distribution of the carbon line emission can be compared with the narrow hydrogen line emission, it might be possible to test the physical association of the C II and H^0 regions. Anantharamaiah, Goss, & Dewdney (1990) have made such a comparison in Orion B. They find that the narrow hydrogen line emission is more localized than the carbon line emission over the continuum source and that both cover only a fraction of the continuum source. Onello et al. (1994) have imaged W48 in 168α emission and have concluded that the H^0 and C II regions are not coextensive. On the other hand, Onello & Phillips (1995) have found a

[1] Joint Astronomy Programme, Indian Institute of Science, Bangalore 560 012, India.

[2] Also at: National Radio Astronomy Observatory, P. O. Box O, 1003 Lopezville Road, Socorro, NM 87801.

strong correlation between the total intensities of the carbon and narrow hydrogen lines in a single-dish observational study of six H II regions. They have concluded that the excitation conditions in the regions from which both lines arise are similar. The main goal of this study is to test this similarity using high-sensitivity and high-resolution VLA observations of carbon and hydrogen recombination lines at 1.4 GHz (168α) from W3A. We present a comparative study of the emission in narrow hydrogen and carbon lines over the face of W3A and discuss the probable physical properties of the partially ionized medium. The continuum emission from W3A and the broad hydrogen recombination line, together with other available data, are used to obtain constraints on the electron temperature, density, and clumpiness in the hot H II region. In this paper, we refer to the broad H 168α lines as H^+ lines, narrow H 168α lines as H^0 lines, the C 168α lines as C^+ lines, and S 168α lines as S^+. The regions in which carbon lines arise are referred to as C II regions.

2. OBSERVATIONS AND RESULTS

W3 was observed in the 20 cm band using the Very Large Array (VLA) in the B configuration for a total of 11 hr spread over three observing sessions in 1993 and 1995. The details of the observations are listed in Table 1. The data were reduced using the AIPS software package developed by NRAO.

The visibility data from different observing sessions were calibrated separately and then combined. The continuum emission was subtracted from the line data by removing a linear baseline determined from the channels free of line emission using the procedure UVLIN in AIPS. After applying natural weighting to the visibilities, continuum and line images were made. The continuum image shown in Figure 1 was made after deconvolving the dirty image using the CLEAN algorithm. Since the continuum source is bright, self-calibration was used to further correct any residual phase errors in both the line and continuum visibilities. A line cube (512 × 512 × 127) was constructed by Fourier transforming the continuum-subtracted and self-calibrated visibility data of all the channels. Only channels that displayed significant line emission were CLEANed to remove the side lobe response. The rms noise in the channel images is ∼1 mJy beam^{-1}. Since the line emission is extended, the line images were smoothed to 10″ × 10″ resolution to increase the signal-to-noise ratio. The rms noise in these images is ∼1.8 mJy beam^{-1} (T_b = 9.8 K).

TABLE 1

OBSERVATIONAL DETAILS

Parameter	Value
Transitions observed	H 168α, C 168α
Rest Frequencies (MHz)	1374.6, 1375.3
Central velocity of observation (km s^{-1})	−60
Central frequency of observation (MHz)	1374.8
Bandwidth (MHz)	1.562 (340 km s^{-1})
Number of channels	127
Spectral resolution (kHz)	12.2 (2.6 km s^{-1})
Observing duration (hr)	
1993 March 20	5
1993 April 09	3
1995 November 22	3
VLA Array Configuration	B
Primary beam (arcmin)	30
Synthesized beam (naturally weighted)	5.″7 × 5.″5, P. A. = 0
Primary flux density calibrator	0134 + 329
Flux density of 0134+329 (Jy)	16.5
Phase calibrator	0212 + 735
Bandpass calibrator	0134 + 329
Phase center	
α(1950)	02^{h}21^{m}49.^{s}0
δ(1950)	61°52′40.″0
rms noise, continuum (mJy beam^{-1})	2 (T_b = 34 K)
rms noise, line (mJy beam^{-1})	1 (T_b = 17 K)

The 20 cm continuum map at a spatial resolution ∼5.″5 of the W3 complex of H II regions in the Perseus arm is shown in Figure 1. The W3 complex consists of eight H II regions labeled A to H, following Wynn-Williams (1971) and Harris & Wynn-Williams (1976). W3A, the largest H II region, is resolved and displays a broken shell morphology, with the shell opening to the south (Roelfsema & Goss 1991). W3C, W3E, W3F, and W3G are unresolved (<6″). W3B is a bright H II region, while W3D and W3H are low-brightness extended H II regions.

The line spectra integrated over the different continuum sources are shown in Figure 2. H 168α line emission is detected from W3A, W3B, W3C + W3D, and W3H, whereas only W3A clearly shows the presence of a C^+ line at a higher frequency. A line to the high-frequency side of the C^+ line is also detected. This could be a C^+ line at a lower velocity (∼ −49 km s^{-1}) or, most likely, an S line at a velocity of ∼ −41.5 km s^{-1}. Since Pankonin et al. (1977) reported the presence of a sulphur line in the W3A spectrum, we assume that this line is indeed S 168α. Gaussians were fitted to the integrated profiles, and the best-fit parameters are listed in Table 2.

TABLE 2

INTEGRATED 168α LINE PROFILES AND CONTINUUM FLUX DENSITIES OF H II REGIONS IN THE W3 COMPLEX

No.	Source	Continuum Flux Density (Jy)	Line	Peak Line S_L (Jy beam^{-1})	V_{lsr} (km s^{-1})	ΔV (FWHM) (km s^{-1})
1.....	W3A	17	H 168α (H^0)	3.6 ± 1.4	−40.2 ± 0.5	7.1 ± 1.5
			H 168α (H II)	2.7 ± 0.5	−42.9 ± 1.3	26.6 ± 3.8
			C 168α	5.3 ± 1.3	−39.7 ± 0.4	5.5 ± 0.9
			S 168α	1.9 ± 1.1	−39.8 ± 1.4	8.0 ± 3.4
2.....	W3B	2.6	H 168α	0.5 ± 0.1	−40.8 ± 0.6	6.3 ± 1.5
3.....	W3C+D	2.9	H 168α	0.6 ± 0.2	−46.6 ± 1.4	22.4 ± 3.8
4.....	W3E	0.05	...	...	...	...
5.....	W3F	0.09	...	...	...	...
6.....	W3G	0.1	...	...	...	...
7.....	W3H	1	...	...	...	...

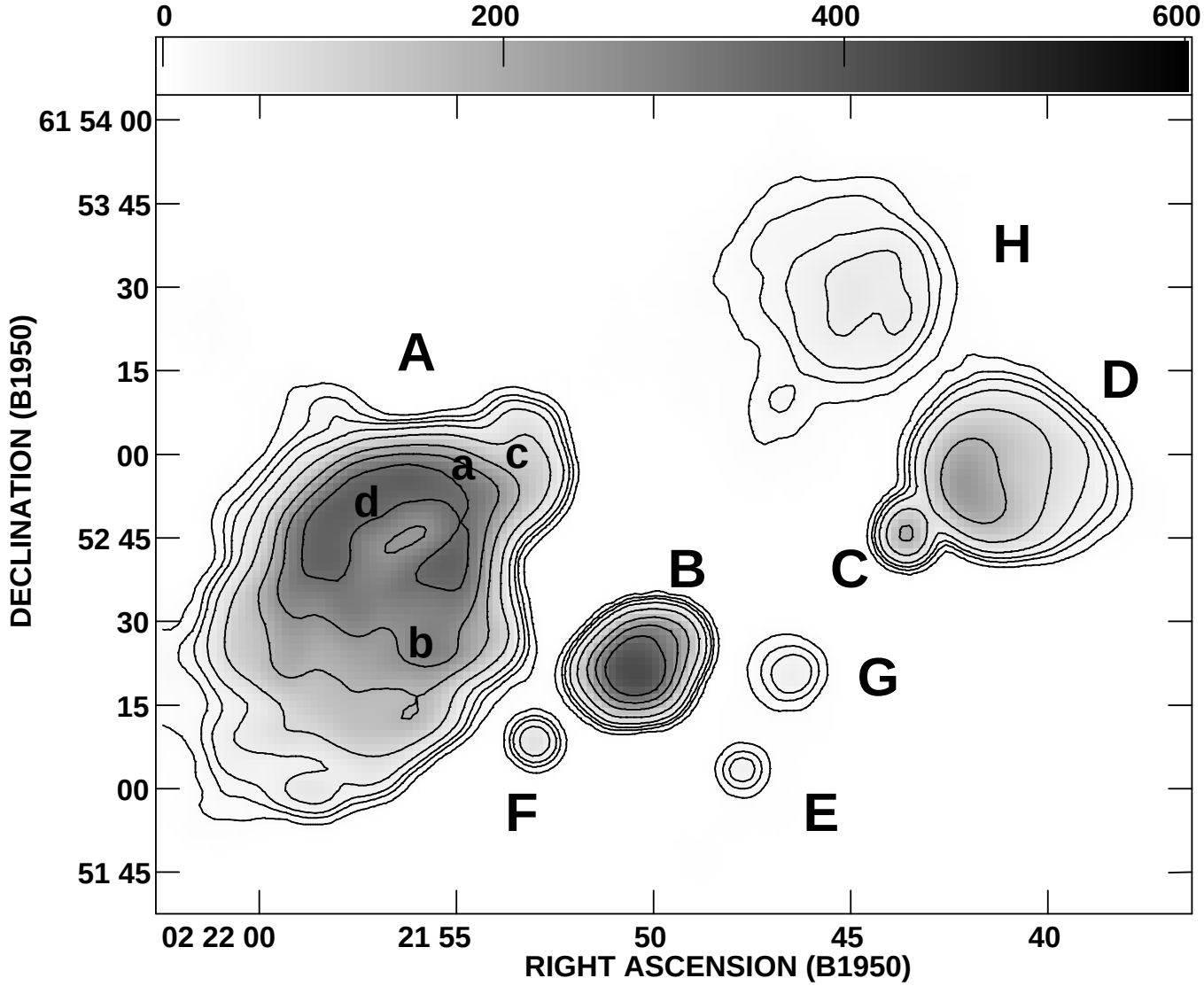

FIG. 1.—Self-calibrated continuum image of W3 (core) near 20 cm, with an angular resolution of 5″.7 × 5″.5, P.A. = −89°. The rms noise in the image is 2 mJy beam^{-1}. Capital letters A to H mark the H II regions in the core region of W3. Lower-case letters a to d mark the positions from which the spectra plotted in Fig. 3 are extracted. The gray-scale range is from 0 to 0.6 Jy beam^{-1}. The contours levels are 1, 2, 3, 5, 10, 20, 30, 40, and 50, in units of 8.5 mJy beam^{-1}.

In contrast to the single-dish observations of Pankonin et al. (1977), the interferometric observations of W3A at 1.4 GHz (e.g., van Gorkom 1980; Roelfsema & Goss 1991) detect a narrow H 168α line that is stronger than the broad H 168α line. This difference is certainly caused by the large beam (∼9′) of the single-dish observation, in which the narrow hydrogen line from W3A is beam-diluted, while the broad line contains contributions from other components of the W3 complex.

Although the primary beam of the VLA at 20 cm (30′) was sensitive to radiation from the entire W3 region, we mainly discuss the emission from W3A, since this is the only H II region from which the carbon line is detected. The remainder of the discussion in this paper, unless specified otherwise, is based on the line and continuum images of W3A with a resolution of 10″.

The line emission displays considerable variation across W3A. Figure 3*a* shows the spectrum at position a in Figure 1, where a weak additional spectral feature at a radial velocity of 17 km s^{-1} is also detected (∼5 σ). The width of this feature is ∼18 km s^{-1}. The gas giving rise to this line is unlikely to be associated with W3A, and most probably is a cloud along the line of sight. Roelfsema (1987) reported a positive-velocity H 166α line from the southern portion of W3A, with a width of ∼22 km s^{-1} centered at about 5 km s^{-1}; this line is not confirmed here. The positive velocity component shown in Figure 3*a* is observed only over a region ∼500 arcsec^2 large in the northern portion of W3A. Emission at a position in W3A where the carbon line intensity exceeds the hydrogen line intensity is shown in Figure 3*b*. The S^+ line is also intense in this region. In Figure 3*c*, the spectrum from the northwest portion of W3A with the broader H line (∼70 km s^{-1}) is shown. The spectrum shown in Figure 3*d* is at the peak of the continuum emission.

In Figure 4*a*, images of the H 168α emission across the continuum shell of W3A are shown at separate velocities. These images contain contributions from both the narrow and broad hydrogen components. The position of the peak in the H 168α emission in W3A shifts with radial velocity.

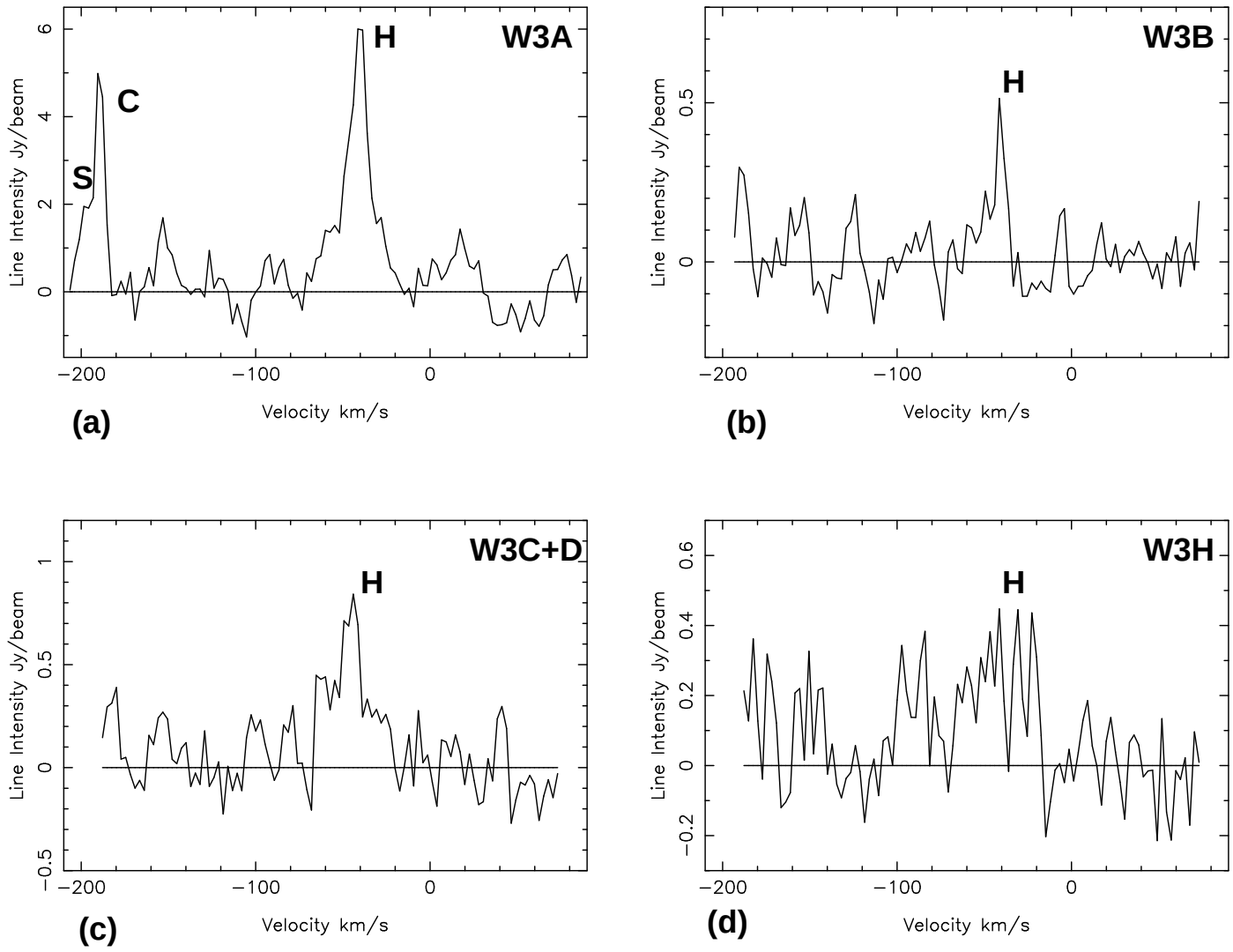

FIG. 2.—Global 168α spectra integrated over the continuum sources: (*a*) W3A, (*b*) W3B, (*c*) W3C + D, and (*d*) W3H

The panels in Figure 4*b* show the C^+ and S^+ intensity distribution over W3A, where the velocities noted in the top right-hand side corner are with respect to the H 168α line. The emission observed at radial velocities of -187.8 and -190.5 km s^{-1} arises from C^+ (add 149.5 km s^{-1} to obtain the absolute velocity), while the emission at velocities near -198.4 km s^{-1} is from S^+ (add 158 km s^{-1} to obtain absolute velocity). The C^+ emission is at least twice the intensity of the S^+ line.

In order to compare the spatial distribution of the H^0 and C II regions, it is necessary to separate the H^0 line from the H^+ line in the images shown in Figure 4*a*, and the C^+ line from the S^+ line in Figure 4*b*. This separation was achieved by fitting four Gaussian components (H^+, H^0, C^+, and S^+) to the line profiles at each pixel in the W3A line cube. The Gaussian fits were made using the procedure PROFIT in the Groningen Image Processing System (GIPSY) (van der Hulst et al. 1992). For the four Gaussians, 12 parameters must be determined. The width of the H^0 line was fixed at 7 km s^{-1}, and the centroid of the H^+ line at -43 km s^{-1}. For S^+, it was only possible to determine the peak amplitude. The width and centroid were held constant at 6.5 km s^{-1} and -197.6 km s^{-1}. These values were determined from the global profile of W3A (Fig. 2*a*) and resulted in stable fits. Gaussians were fitted to the spectra only where the continuum intensity exceeded 400 mJy beam^{-1} in the 10″ image. The above procedure generated spatial distributions of the peak intensity, widths, and centroids of the 168α line emission of W3A shown in Figures 5*a*, 5*b*, and 5*c*.

Figure 5*a* shows that in addition to the H^0 and C^+ lines, the H^+ and H^0 lines are also dissimilar. The S^+ and C^+ lines show similar morphologies. As expected, the H^+ line has the same shape as the continuum of W3A; this line arises from the H II region. The C^+ emission has peaks in the southwest and northwest regions of W3A. An enhancement in the C^+ emission is also observed in the northwest region of the source, where W3A is probably breaking out of the parent molecular cloud (Roelfsema et al. 1987). The peak emission of the H^0 line is also seen in the same region.

Figure 5*b* shows the distributions of radial velocities of the H^0 and C^+ lines. No correlation is observed. The velocity of the H^0 line shows a gradient across W3A, with higher velocities to the south. The C^+ velocities are uniform over the source to within 2.5 km s^{-1}. The distribution of widths of the observed H^+ and C^+ lines over W3A are shown in Figure 5*c*. The width of the C^+ line varies from 4 km s^{-1} in the north to 10 km s^{-1} in the southeast. The width of the H^+ component varies between 15 and 70 km s^{-1} across

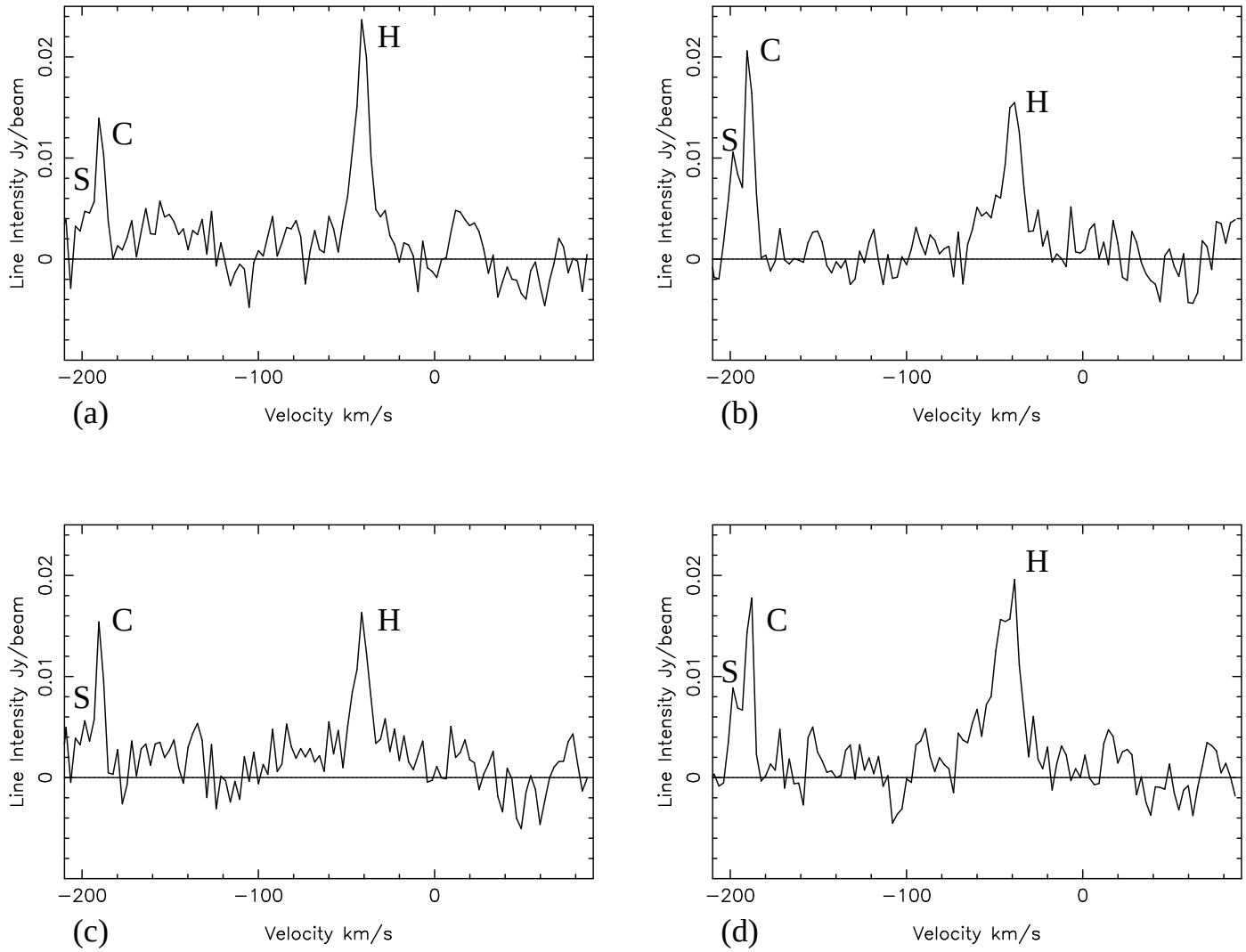

FIG. 3.—Spectra at four typical pixels in W3A. The velocity scale is based on H 168α. (*a*) Spectrum at a typical position to the north of W3A, where a line at velocity ~ 17 km s^{-1} is detected. (*b*) Spectrum at a typical position in the south of W3A, where the carbon line is more intense than the hydrogen line. (*c*) Typical spectrum to the northwest of the continuum source where the broadest (~ 70 km s^{-1}) hydrogen lines are observed. (*d*) Spectrum at the continuum peak.

W3A with the widest (~ 70 km s^{-1}) lines originating to the north. The increased widths of the H^+ line that we observe toward the northwest supports the suggestion by Dickel, Harten, & Gull (1983) and Roelfsema et al. (1987) that the H II region is expanding into a tenuous medium.

Figure 6 shows the distribution of the line-to-continuum ratio, S_l/S_c, for the H^+, H^0, and C^+ lines. The ratio is expected to be uniform if the H II region is responsible for both the line and continuum emission. Alternatively, the ratio would be uniform if the line-producing gas was homogeneous and stimulated emission of the background radiation were the main emission mechanism. Any structure displayed by the emission in the second case could be produced by variation in the physical properties of the foreground gas. The line-to-continuum ratio of the H^+ line is nearly constant over the source. The widths (~ 27 km s^{-1}) of these lines and the uniform ratio S_l/S_c seem to indicate that the line and the thermal continuum arise in the same hot gas. However, the distribution of the line-to-continuum ratio of the H^0 and C^+ lines over the continuum source exhibit structure (see Figs. 6*b* and 6*c*). Since stimulated emission is important in the formation of the intense narrow lines, this structure is caused by varying physical properties of the foreground partially ionized gas. The ratio S_l/S_c of the H^0 line peaks to the northwest of W3A and decreases along a ridge that runs to the southeast. Regions of decreased S_l/S_c are observed in the northeast and southwest. Enhancement in C^+ is also observed toward the northwest edge. Moreover, C^+ emission peaks in the regions south of the center of W3A. A minimum in the S_l/S_c is observed to the northwest of the center of W3A.

3. THE PARTIALLY IONIZED MEDIUM

The H^+ line emission arises in the classical H II region, W3A. However, the widths of the H^0 and C^+ lines rule out their origin in the H II region; the lines originate in the partially ionized medium associated with the H II region (Palmer et al. 1967; Pankonin et al. 1977). Owing to their different ionization potentials, hydrogen (13.6 eV) is likely to be partially ionized while carbon (11.4 eV) could be fully ionized in this gas. Since the H II region is optically thick at 20 cm ($\tau \sim 2.3$ at the continuum peak), the C^+ and H^0 lines can only arise from the gas in front of the H II region.

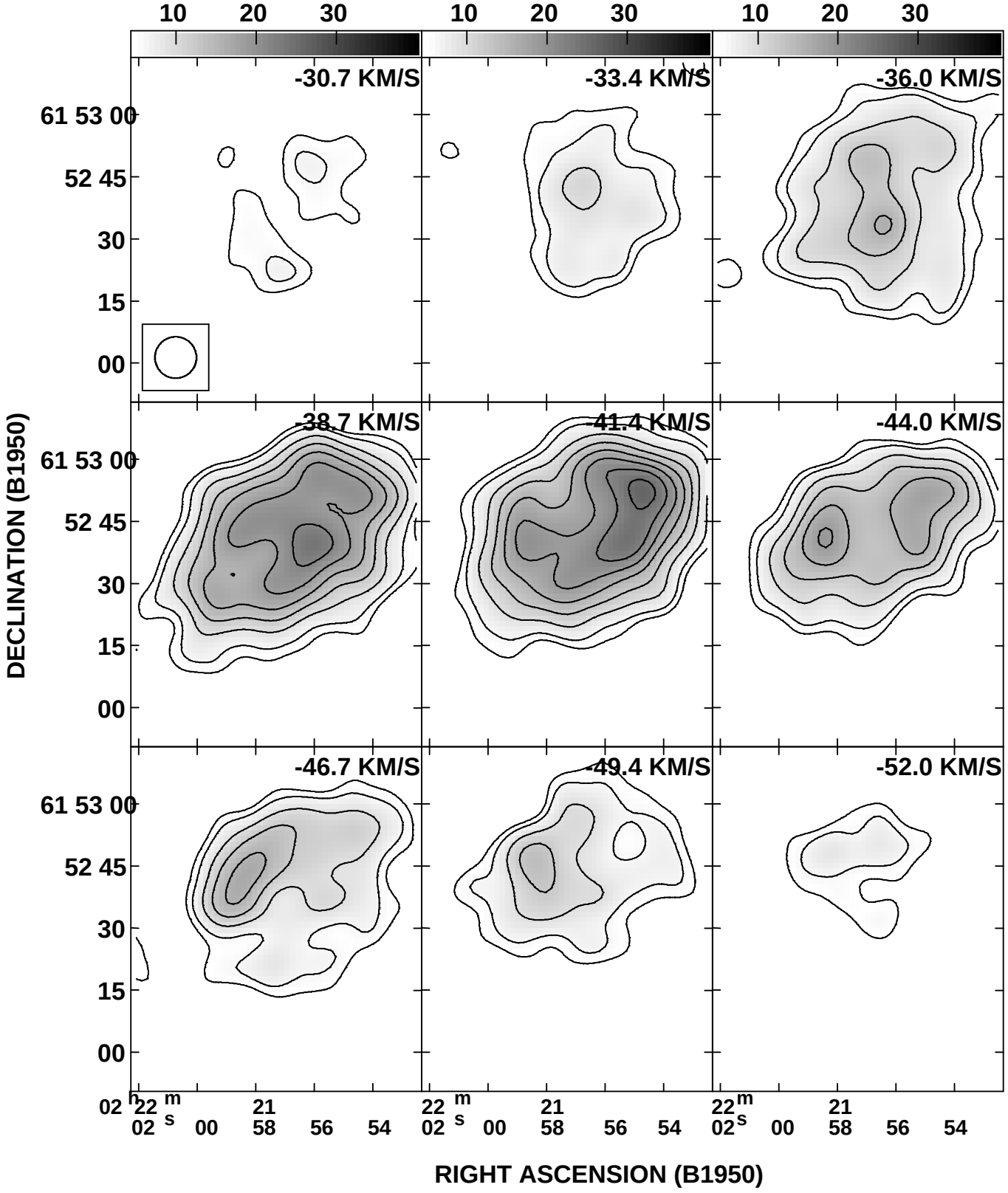

FIG. 4*a*

FIG. 4.—(*a*) Distribution of H 168α across W3A at radial velocities ranging from -31 to -52 km s^{-1}, with an angular resolution of 10″. Each panel is separated by 2.6 km s^{-1}, which is the spectral resolution. Contributions from both the narrow and broad components are included. The gray-scale flux range is 5 to 40 mJy beam^{-1}. The contour levels are 1.5, 2, 3, 4, 5, 6, 7, 8, 9, and 10, in units of 3 mJy beam^{-1}. (*b*) Distribution of C 168α and S 168α across the continuum source in W3A. The radial velocities are labeled with respect to the H 168α line. To obtain the radial velocity of the C 168α line add 149.5 km s^{-1}, and for the S 168α add 158 km s^{-1}, to the values noted in the top right-hand side corner of each panel. Strong carbon line emission is observed at velocities of -187.8 and -190.5 km s^{-1}. The emission at -198.4 km s^{-1} is due to S 168α. The gray-scale coding and contour levels are as in Fig. 4*a*.

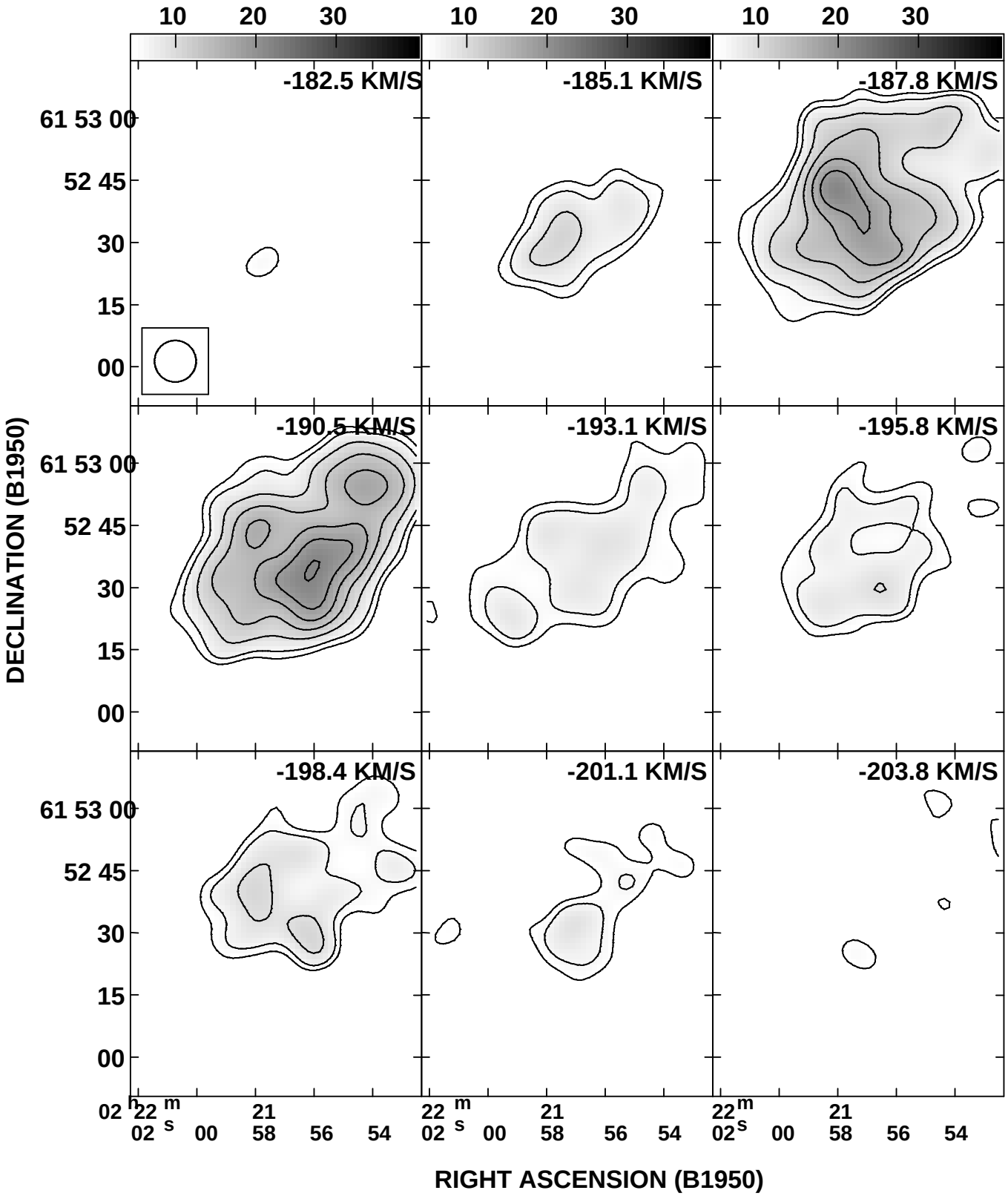

FIG. 4*b*

3.1. *Spatial Distribution of* H^0 *and* C^+ *Line Regions*

If the narrow lines arise in a homogeneous, isothermal, partially ionized layer in front of the H II region, then the distributions traced by the C^+ and H^0 lines should resemble the continuum distribution arising from stimulated emission (Pankonin et al. 1977). Since the distributions do not mimic the continuum (Fig. 5*a*), the structure observed in the C^+ and H^0 lines can only be explained by variations in the physical conditions (n_e, T_e, or emission measure) of the foreground gas (see also Roelfsema et al. 1987). Furthermore,

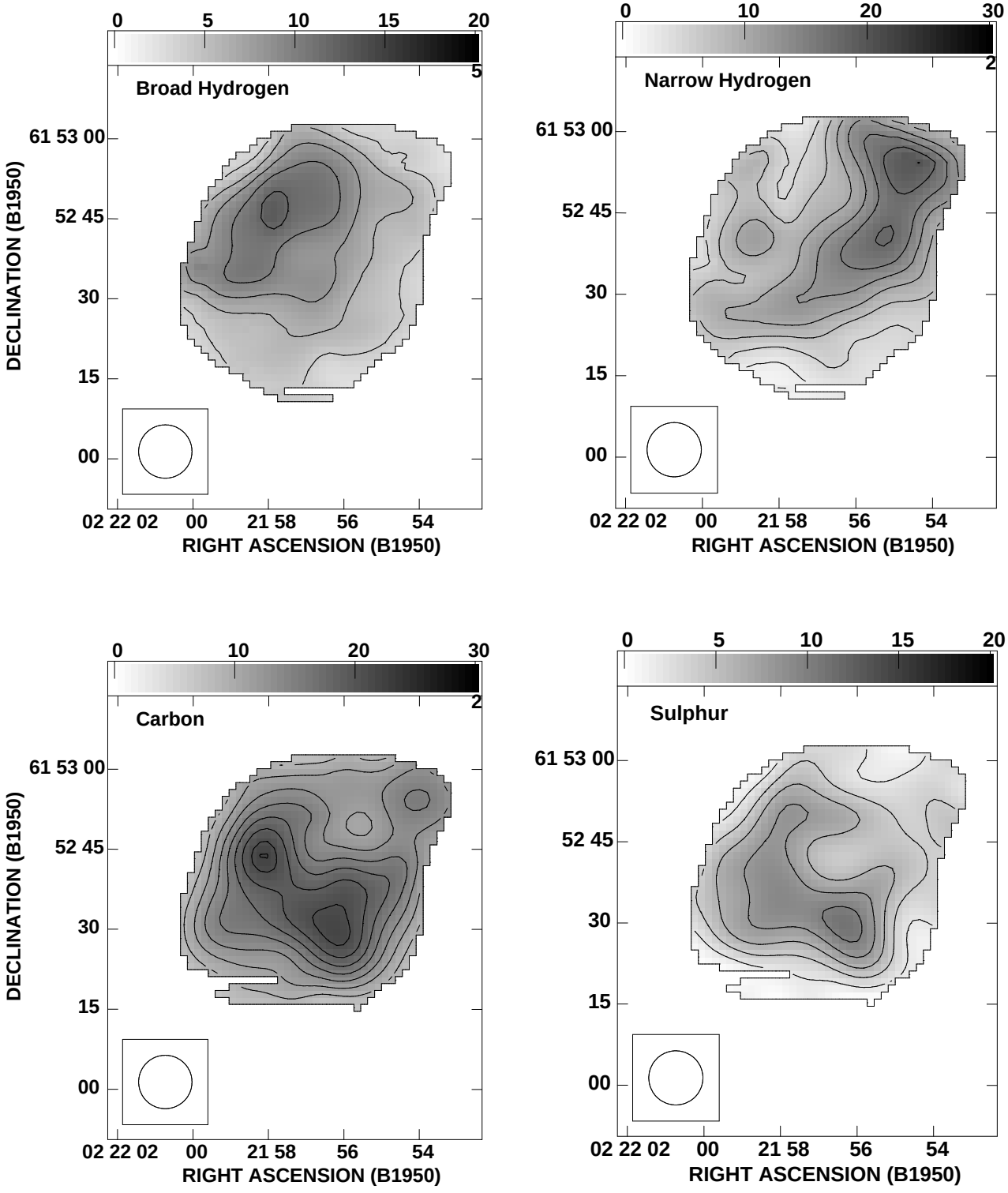

FIG. 5*a*

FIG. 5.—(*a*) Peak intensity distribution of H^+, H^0 , C^+, and S^+ across W3A obtained from Gaussian fits to the emission at each pixel. The gray-scale range in the images is 0–20 mJy beam^{-1} for the H^+, 0–30 mJy beam^{-1} for the H^0, 0–30 mJy beam^{-1} for the C^+ line, and 0–20 mJy beam^{-1} for the S^+ line distribution. The contour levels for the H^+ line are 4, 6, 8, 10, and 12 mJy beam^{-1}, and for the H^0 line they are 2.5, 5, 7.5, 10, 12.5, 15, 17.5, and 20 mJy beam^{-1}. The contours for the C^+ line are 9, 11, 13, 15, 17, 19, 21, and 22 mJy beam^{-1}, and for the S^+ line they are 2, 4, 6, 7, and 10 mJy beam^{-1}. (*b*) The distribution of radial velocities of the H^0 and C^+ lines. The gray-scale flux range is -45 to -35 km s^{-1} for the H^0 and -195 to -185 km s^{-1} for the C^+ distribution. The contours are drawn from -42 to -37 km s^{-1} at intervals of 1 km s^{-1} for H^0 and from -190.5 to -188.5 km s^{-1} at intervals of 0.5 km s^{-1} for C^+. The velocities are with respect to the rest frequency of the hydrogen recombination line. (*c*) The distribution of the widths of the H^+ and C^+ lines across W3A. The gray scale is 10–80 km s^{-1} for H^+ and 2–13 km s^{-1} for C^+. The contours levels are 15, 20, 22, 24, 26, 28, 30, 35, 40, 45, 50, 60, and 70 km s^{-1} for H^+ and 4, 5, 6, 7, 8, 9, and 10 km s^{-1} for C^+.

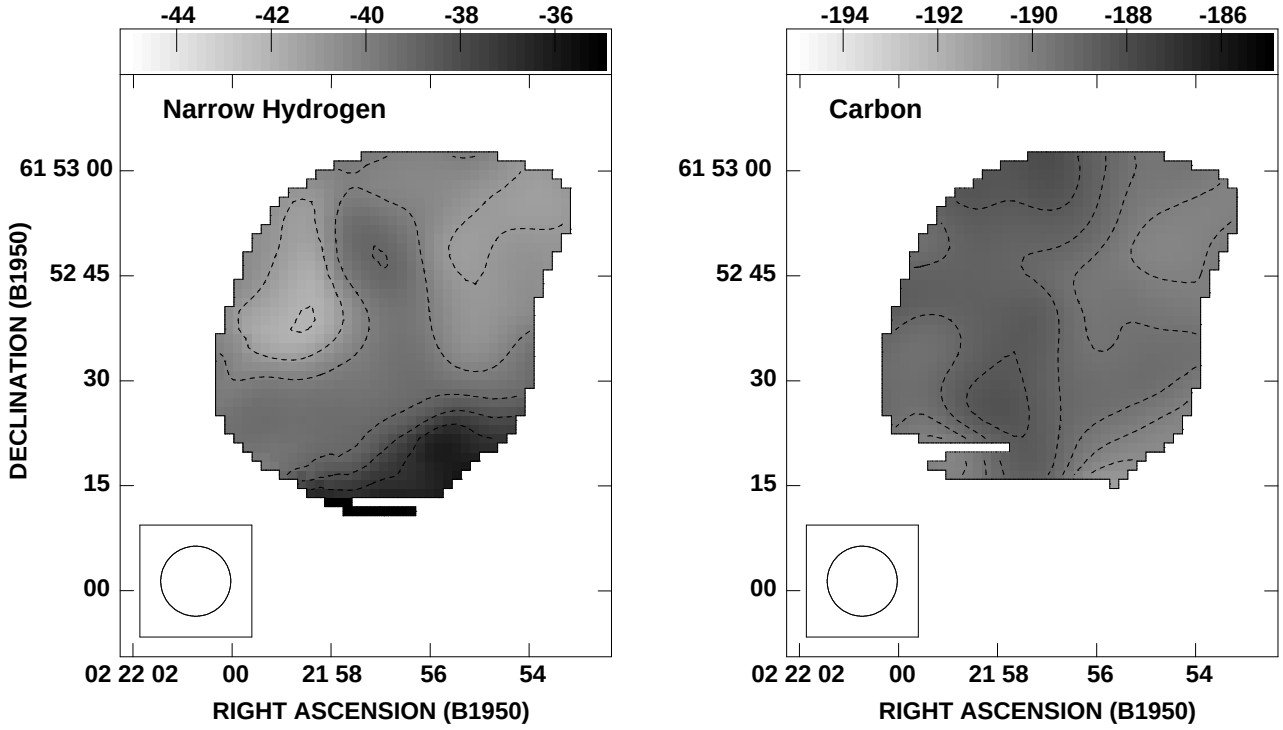

FIG. 5*b*

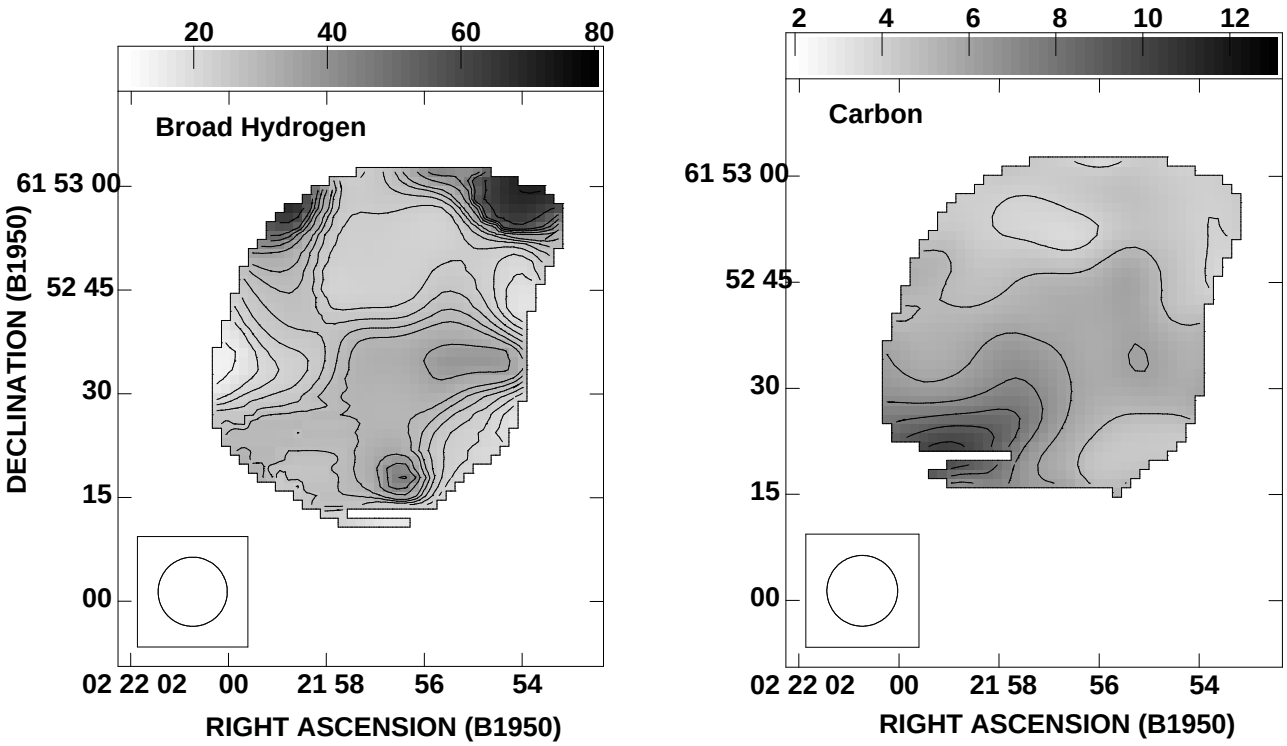

FIG. 5*c*

since the distributions traced by the C^+ (Fig. 6*c*) and the H^0 (Fig. 6*b*) lines over W3A are themselves different, this suggests that the H^0 and C II regions are not identical. However, the correlation observed between the two distributions near the northwest edge and along the ridge extending to the southwest (see Figs. 6*b* and 6*c*) suggests some common origin. Line-to-continuum ratios of C^+ are in the range of 0.01–0.02. Large values ($\sim$0.03) occur to the northwest. Small ratios for the H^0 line (0.005–0.015) are observed over W3A. A peak of $\sim$0.03 is found to the northwest. Typical S_l/S_c for C^+ is about twice that of the H^0. Moreover, strong C^+ line emission is observed over the entire continuum source; the H^0 line is essentially confined to a ridge running across the source (see Fig. 6). These

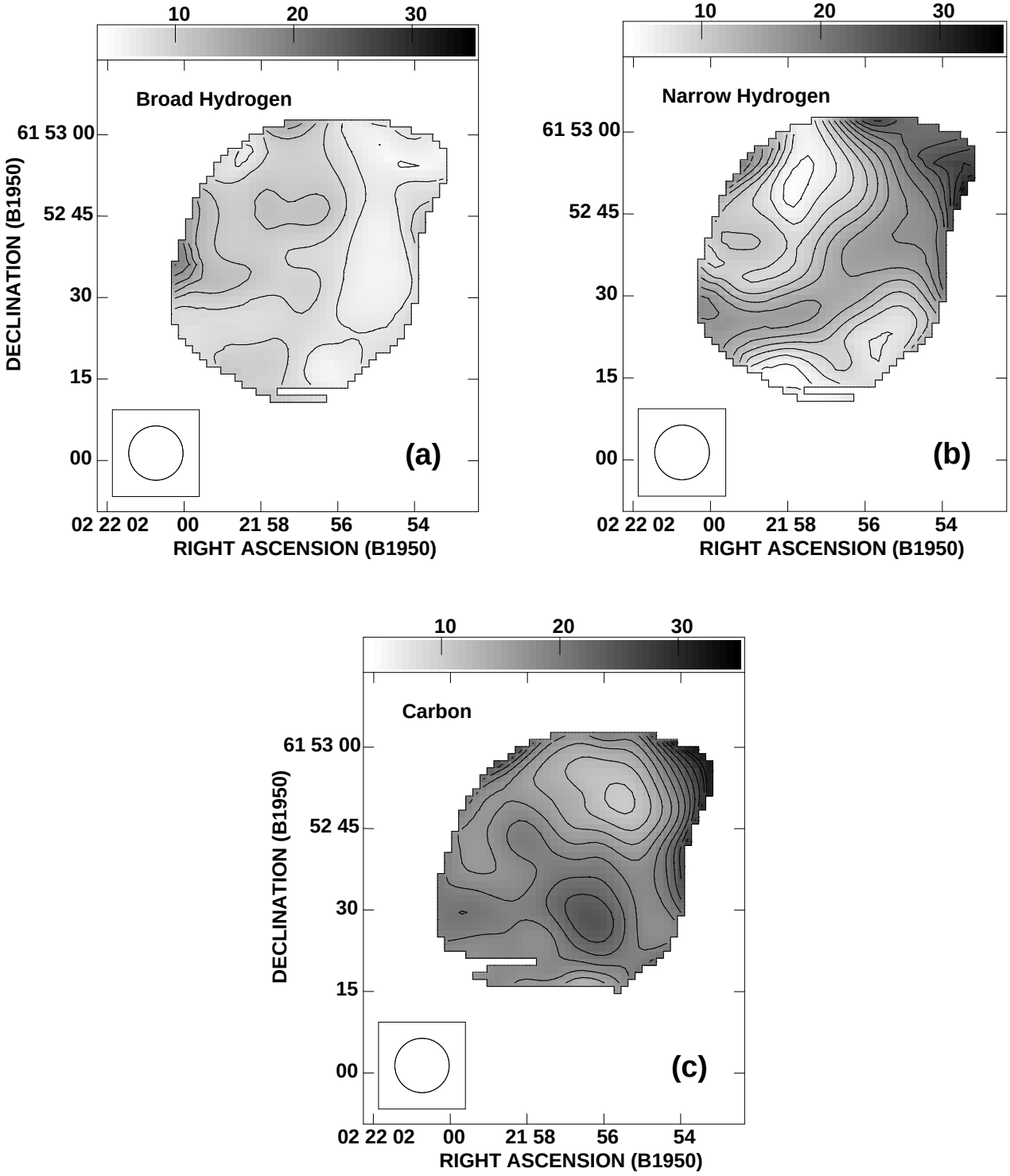

FIG. 6.—Distribution of the line-to-continuum ratios of (*a*) H^+, (*b*) H^0, and (*c*) C^+ lines over the continuum source. The gray-scale flux range is 4×10^{-3} to 35×10^{-3}. The contour levels are from 5 to 29, drawn at intervals of 2 in units of 1×10^{-3}.

differences suggest a structure in which the H^0 line is emitted only from a thin, patchy layer of partially ionized medium (PIM) just outside the H II region. The C^+ line, on the other hand, is emitted from both this region and the photodissociation region (PDR) (Tielens & Hollenbach 1985). In the PDR, the stellar ultraviolet radiation field (6–13.6 eV) is sufficient to keep carbon (11.4 eV) ionized, but is not strong enough to ionize hydrogen (13.6 eV). Thus, since carbon is likely to be fully ionized to greater depths in the neutral gas compared to the partially ionized hydrogen region, the H^0 line would be weaker and is expected to have a different spatial distribution.

Anantharamaiah et al. (1990) have imaged the H II region Orion B in the H^0 and C^+ lines; they infer that the C^+ and H^0 regions are spatially coincident, confined to a small area of the continuum source. In addition, Anantharamaiah et al. (1990) find the C^+ emission to be more widely distributed over Orion B than the H^0 emission. Thus, W3A is

quite different; the two line distributions are dissimilar and do cover almost the entire source W3A. Furthermore, in Orion B, the S^+ distribution is distinct from that of C^+, whereas in W3A, the C^+ and S^+ emission are essentially identical. Thus, the partially ionized gas in the vicinity of these two classical H II regions display distinct properties. However, our results for W3A match those for W48. Onello et al. (1994) have imaged the H II region complex W48 in 168α emission and detected H^+, H^0, C^+, and S^+ lines from W48A. They find from their high-resolution imaging that the C^+ and S^+ line distributions over W48A are identical, but H^0 has a distinct structure. Onello et al. (1994) conclude that the gas responsible for the H^0 line is not coextensive with the C II region.

3.2. *Expansion to the Northwest of W3A*

As discussed in § 3.1, an enhancement in the line-to-continuum ratio is observed in the H^0 and C^+ lines toward the northwest part of W3A. Roelfsema et al. (1987) had noted the excess C^+ emission from this region and attributed the enhanced emission to ultraviolet photon leakage from the H II region. Dickel et al. (1983) also noted strong [O III] emission from this region, which requires a large intensity of ultraviolet photons, and suggested that the H II region W3A may be in the process of breaking out of its parent molecular cloud in this region. Roelfsema et al. (1987) suggest that in this region the H II has become density-bound and that the relatively hard radiation field would lead to increased ionization in the surrounding carbon cloud and hence stronger spontaneous C^+ emission. We observe enhanced H^0 emission in addition to C^+ emission from this region. The increased fractional ionization of hydrogen in the PIM also seems to be producing this enhancement. Furthermore, we find that the H^+ lines observed from this region are wider than in the remainder of the source, as seen in Figure 5*a*, again providing evidence for expansion. The central velocities of the H^0 (-41 km s^{-1}) and C^+ (-40.5 km s^{-1}) lines are slightly more negative in this region compared to most of the source, supporting the hypothesis (Roelfsema et al. 1987) that the gas in this region is approaching the observer.

3.3. *Comparison with Other Molecular- and Ionized-Gas Tracers*

We have compared the recombination-line distribution with the optical depth maps of H_2CO, which trace the H_2 molecular gas. The H_2CO absorption lines sample the dense molecular gas on the near side of the H II region and hence are likely to be associated with the gas that gives rise to the narrow recombination line emission. Dickel, Goss, & Condon (1996) have imaged W3A in the 6 cm and 2 cm transitions of H_2CO; they find enhanced opacities in the southwest of W3A in both the transitions at -39.4 km s^{-1}. The southwest region overlaps with the region where a peak in the optical depth of the C^+ line is observed near -41 km s^{-1}. Absence of a similar increase in the H^0 line emission in this region suggests that the enhanced C^+ emission in this region is associated not with the PIM but rather with the molecular clumps in the PDR. Furthermore, H_2CO displays a low optical depth in the northern region at -40.5 km s^{-1}, which coincides with the minimum seen in the C^+ emission in the line-to-continuum ratio in Figure 6*c*. In § 3.2, it was shown that a fraction of C^+ emission originates in the PIM. The similar structure of the C^+ and the H_2CO indicates that the remaining part of the C^+ line emission must arise in the PDR.

We also searched for any possible correlation between the C 168α and the [C II] 158 μm fine-structure emission in W3A. Both of these lines involve ionized carbon. Moreover, the process of dielectronic-like recombination (Watson, Western, & Christensen 1980, hereafter WWC80) which significantly modifies the electronic level populations in carbon, is an exciting mechanism for the fine-structure transition. The W3 region has been imaged in the 158 μm line by Howe et al. (1991) with a resolution of 55″. Unlike the C 168α line emission, the 158 μm line emission is detected from the entire W3 complex, with enhanced emission near W3B. No increase in the 158 μm line emission is seen near W3A, in contrast to the C 168α line. This difference seems to indicate that the predominant contribution to the two lines may be from different components. However, strong C 92α emission has been detected from W3B by Adler, Wood, & Goss (1996), which follows the trend of the fine-structure emission. Heiles (1994) has suggested that the observed Galactic [C II] fine-structure emission arises in an extended low-density warm ionized medium (ELDWIM), while the cold neutral medium (CNM) and PDR are the sites of origin for the [C II] 158 μm line, in decreasing order of importance. No correlation is observed between the C 168α line from W3A and the fine-structure emission with the existing resolution. High angular resolution [C II] 158 μm data are required to further investigate the origin of these two species of lines.

No meaningful comparison between the C^+ and H^0 lines and the 21 cm H I absorption (van der Werf & Goss 1990) could be made, since the 21 cm line toward W3A at a radial velocity of ~ -40 km s^{-1} is saturated.

3.4. *Modeling* H^0 *and* C II *Regions*

The extensive range of physical conditions that can explain the C^+ and H^0 observations can be constrained by making simplifying assumptions as follows:

1. *Limits on the electron densities from molecular densities.*—Typical densities of $\sim 10^5$ cm^{-3} have been derived for the foreground molecular material in W3A from H_2CO observations (Dickel et al. 1996). Hence, the atomic hydrogen densities in the PIM and PDR cannot be in excess of $\sim 2 \times 10^5$ cm^{-3}, since these regions are formed from the dissociation of H_2 molecules. For the C II region, if the number abundance of carbon with respect to hydrogen is assumed to be 3×10^{-4} and if all the electrons are believed to come from ionization of carbon, then the electron density cannot exceed ~ 60 cm^{-3}. If carbon is depleted onto dust grains, then this limit will be lowered. In the H^0 region, the electrons may be contributed by both carbon and hydrogen; thus, the electron densities may exceed 60 cm^{-3}. If electron densities of 10–30 cm^{-3} are contributed by hydrogen (implying a fractional ionization for hydrogen of $\sim 10^{-4}$), then the upper limit on the electron density would be ~ 80 cm^{-3}. Thus, we assume that the electron densities are in the range 1–60 cm^{-3} for the C II region and 1–80 cm^{-3} for the H^0 region.

2. *Limits on the thickness of the foreground PIM region.*—Roger and Dewdney (1992) have shown for a spherically symmetric H II region excited by an O5 star that the surrounding dissociation region will extend to a maximum of 1.5 times the size of the H II region and that the

size increases as the spectral type becomes later. The central star in W3A is believed to be of type O6 (Adler et al. 1996). If we assume that W3A is spherically symmetric with uniform density, then since its linear size is $\sim$0.4 pc, we obtain a diameter of $\sim$0.6 pc for the dissociation (H^0 and H I) zone. Hydrogen is likely to be partially ionized in a part of this photodissociation zone, and hence this value is an upper limit for the H^0 region. However, since the C II region is associated with both the H^0 and the H_2 regions, the Roger-Dewdney limit is not applicable to its size.

The width of the H^0 line places an upper limit of 1000 K on the electron temperature of the partially ionized gas. Moreover, if the two lines (H^0 and C^+) are assumed to arise in gas with similar properties, then the widths of the two lines imply a temperature of $\sim$400 K. Since the electron temperature is quite uncertain, we have modeled the regions for temperatures of both 100 K and 1000 K. Based on these temperatures and the constraints on the density and size of the emitting region, we consider two types of models for the C II and H^0 regions: (1) spontaneous emission and (2) stimulated emission arising from the strong thermal background radiation field from the H II region. In order to calculate the background continuum radiation, the emission measure and temperature of the H II region were taken to be 1.3×10^7 pc cm^{-6} (Adler et al. 1996) and 9000 K, respectively. Since the narrow 168α line–emitting region lies in front of the H II region, the dilution for the background radiation is at least 0.5; we assume a dilution factor of 0.5.

Even though there are obvious inhomogeneities in the line distribution, we have assumed an isothermal, homogeneous line-producing cloud to simplify the modeling process. The line emission at the continuum maximum (6 mJy beam^{-1} for the H^0 line and 21 mJy beam^{-1} for the C^+ line) was used to constrain the emission measure for various assumed values of n_e in the narrow line–emitting regions. The observed variation in line emission across the source is assumed to arise from either a variation in path lengths through the gas or a variable electron density. The departure coefficients b_n and β_n, which are a measure of the deviations of the level populations from LTE, were calculated using the computer code of Salem & Brocklehurst (1979), modified by Walmsley & Watson (1982) to include the effects of dielectronic-like process (WWC80) and further modified by Payne, Anantharamaiah, & Erickson (1994) to extend the calculation to large quantum numbers ($n_{max} \sim$ 10,000). The process of dielectronic-like recombination significantly modifies the level populations in carbon and is most effective in regions where the free electron energies exceed 0.0078 eV ($\sim$92 K) (WWC80). This process involves the excitation of the fine-structure transition ($^2P_{1/2} \rightarrow {}^2P_{3/2}$) in the ground state of carbon by the recombining energetic electron. The radiative transfer equation was solved for $T_e = 100$ and 1000 K with n_e ranging from 1–60 cm^{-3} for the C II region and 1–80 cm^{-3} for the H^0 region. The resulting emission measure and path length through the gas required to explain the observed line emission at the continuum maxima for $T_e = 100$ and 1000 K and three values of n_e are listed in Table 3.

If $T_e = 100$ K and $n_e = 80$ cm^{-3}, the spontaneous emission models require path lengths of 0.1 pc through the H^0 region. The remaining spontaneous emission models for the H^0 region, listed in Table 3, are ruled out by the Roger-Dewdney limit. The models, which include contributions from stimulated emission, can explain the observed H^0 line from W3A if $n_e = 10$–80 cm^{-3} for all temperatures between 100 and 1000 K without violating the Roger-Dewdney limit. Moreover, $T_e = 100$ K, $n_e = 1$ cm^{-3} can also explain the observed line intensity. On the other hand, for any density between 10 and 80 cm^{-3} and temperature in the range $T_e = 100$–1000 K, both the spontaneous and stimulated emission models for the C II region require reasonable path lengths. In addition, the stimulated emission model with $T_e = 100$ K and $n_e = 1$ cm^{-3} can also explain the observed C^+ line intensity. The remaining spontaneous emission models require extremely long path lengths (almost 50–30,000 times the size of the dissociation zone calculated by Roger & Dewdney 1992), which appears unlikely even for the C II regions.

Since we have narrow recombination line data at only one frequency, we are unable to tightly constrain the physical parameters of the H^0 and C II regions. From the above analysis, we can say that both the H^0 and C II regions can have a temperature in the range of 100–1000 K. The electron densities in H^0 can be between 10 and 80 cm^{-3}, whereas in the C II region the range is 10 to 60 cm^{-3}. However, carbon is expected to be depleted onto grains, and hence the upper limit on the electron density will be lower than 60 cm^{-3}.

4. THE H II REGION W3A

4.1. *Electron Temperature*

At frequencies where a fully ionized H II region becomes optically thick ($\tau > 1$), the measured continuum brightness temperature approaches the electron temperature of the gas (Shaver 1969; Osterbrock 1989, p. 165), the two differing by a small correction factor introduced by the finite optical

TABLE 3

PHYSICAL PARAMETERS OF THE H^0 AND C II REGIONS IN W3A

			ONLY SPONTANEOUS EMISSION				SPONTANEOUS + STIMULATED EMISSION			
			100 K		1000 K		100 K		1000 K	
No.	Line	N_e (cm^{-3})	EM (pc cm^{-6})	L (pc)	EM (pc cm^{-6})	L (pc)	EM (pc cm^{-6})	L (pc)	EM (pc cm^{-6})	L (pc)
1.....	H 168α	1	390	390	9600	9600	1	1	55	55
		10	390	4	9900	99	2	0.02	65	0.7
		80	810	0.1	17800	3	15	0.002	270	0.04
2.....	C 168α	1	530	530	16700	16700	5	5	270	270
		10	780	8	25000	250	9	0.09	490	5
		60	2200	0.6	45000	12	110	0.03	1550	0.4

depth. Therefore, in the case of W3A, which appears to be optically thick at 20 cm, the measured brightness temperature differs from the physical temperature of the cloud as

$$T_b = T_e(1 - e^{-\tau_c}) \, . \quad (1)$$

The optical depth can be derived if a continuum image at a higher frequency where the H II region is optically thin is available, using the method described by Subrahmanyan & Goss (1996). Based on a comparison of the 8.3 GHz image published by Adler et al. (1996) with the image at 1.4 GHz (see Fig. 7*a*), we can calculate the electron temperature. From the nature of the one-dimensional crosscuts across these images through the continuum peak (Fig. 7*b*), it is clear that the H II region is becoming optically thick near 20 cm ($\tau \sim 2.3$ at continuum peak). Using the peak brightness

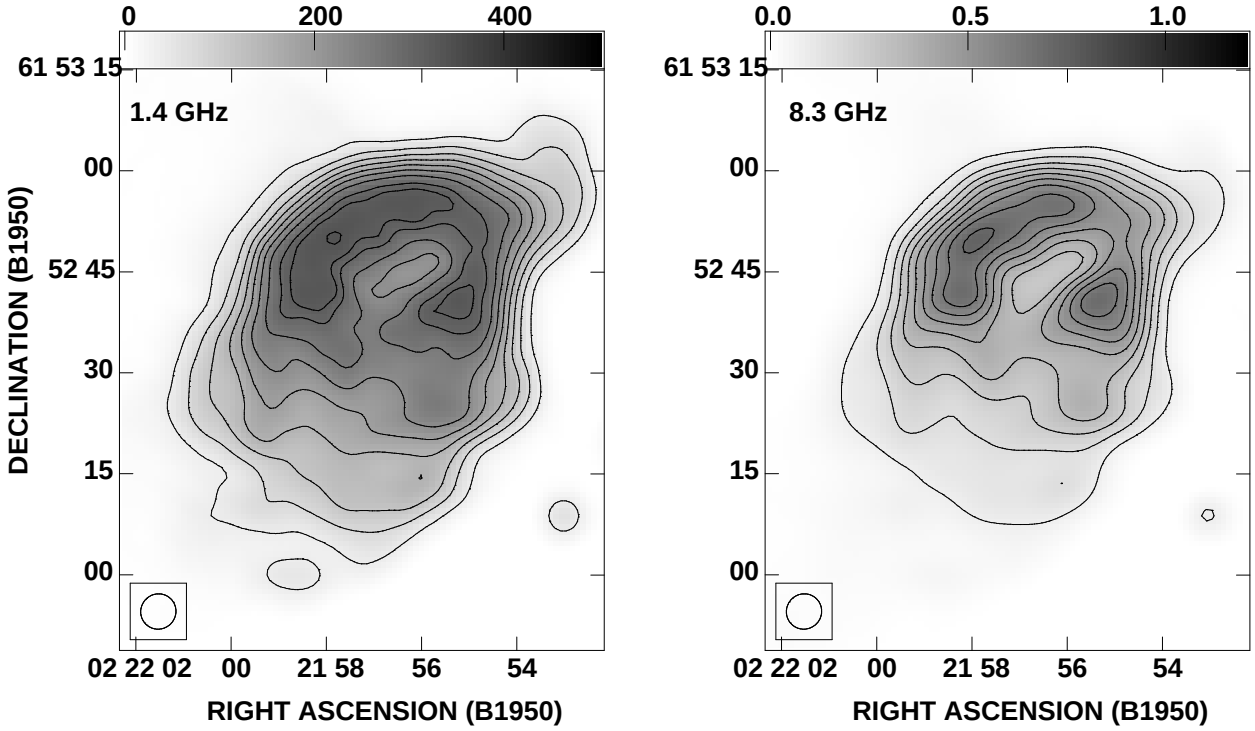

FIG. 7*a*

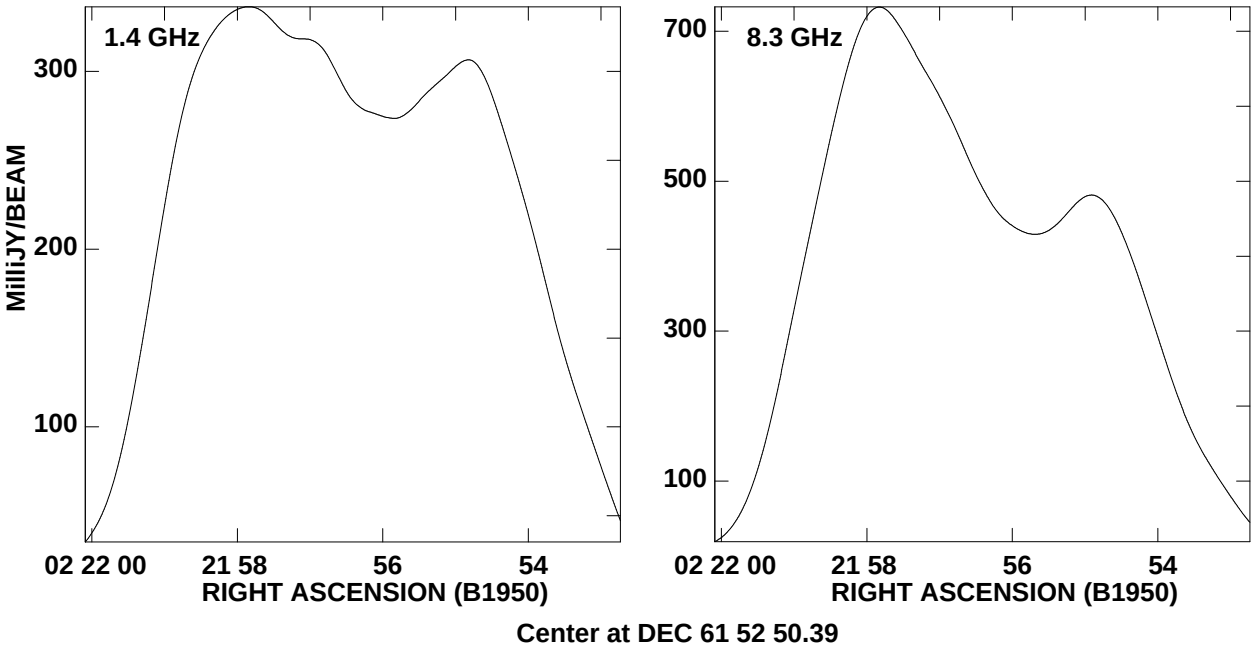

FIG. 7*b*

FIG. 7.—(*a*) Continuum distribution in W3A at 1.4 GHz and 8.3 GHz at a resolution of 5″.2. The gray scale range is 0–0.5 Jy beam^{-1} in the 1.4 GHz image and 0–1.2 Jy beam^{-1} in the 8.3 GHz image. The contour levels are 1 to 10, drawn at intervals of 1, in units of 37 mJy beam^{-1} in the 1.4 GHz image and in units of 79 mJy beam^{-1} in the 8.3 GHz image. (*b*) Crosscuts across the continuum images of W3A at 1.4 and 8.3 GHz through the position of maximum intensity. The intensity scale is in mJy beam^{-1}. The conversion factor to T_b at 20 cm is from 30 K (mJy beam^{-1}).

determined at 1.4 GHz and 8.3 GHz from Figure 7*a*, we calculated an electron temperature of 8760 ± 215 K (using the method described by Subrahmanyan & Goss 1996). From the line-to-continuum ratio of the H 92α (8.3 GHz) line, Adler et al. (1996) obtained a temperature of 7970 ± 140 K. Since W3A is optically thin at 8.3 GHz, the H 92α line samples the entire line of sight; the emission is expected to be dominated by the central regions that have the highest emission measures. On the other hand, the temperature from the optically thick brightness at 20 cm is likely to be characteristic of the outer regions of the H II regions. Adler et al. (1996) compared the T_e of W3A obtained from three different methods, including the method we have used here, and concluded that there is some suggestion of a radial gradient in the electron temperature of W3A, but only at the 3 σ level.

4.2. *Electron Density and Filling Factor*

If the H II region W3A is assumed to be a homogeneous spherical cloud, then the observed continuum flux density at a frequency at which the region is optically thin can be related to the average electron density in the region. The continuum flux density of W3A at 8.3 GHz obtained from the image in Figure 7*a* is 23 Jy, and the angular size is ∼50″. Taking $d = 2.4$ kpc and $T_e = 9000$ K, we obtain $n_{e,\mathrm{rms}} = 2200\ \mathrm{cm}^{-3}$, using the formula given by Mezger & Henderson (1967). This is a lower limit to the true electron density in W3A, since the intensity distributions in Figure 7*a* indicate density enhancements.

Pressure broadening is a sensitive function of the principal quantum number n and the true electron density $n_{e,\mathrm{true}}$. Hence, if a pressure-broadened recombination line can be observed from the H II region W3A, then the $n_{e,\mathrm{true}}$ in that region can be estimated. Using this $n_{e,\mathrm{true}}$ and the $n_{e,\mathrm{rms}}$, the filling factor of the H II region can be estimated. Simultaneously with an attempt to detect ^{3}He at 8.6 GHz, Uson & Goss (J. M. Uson & W. M. Goss 1997, private communication) have observed the H 171η line from W3A (see Fig. 8). The line has a central velocity of ∼ −28 km s^{-1}, a width of ∼77 km s^{-1}, and a line-to-continuum ratio of (7 ± 1) × 10^{-4}. If we assume that this line arises in the H II region W3A and that it is pressure broadened, then the line width translates to a true electron density of 2×10^4 cm^{-3}.

The clumpiness in a medium is characterized by the filling factor, which is defined as $\epsilon = (n_{e,\mathrm{rms}}/n_{e,\mathrm{true}})^2$. From $n_{e,\mathrm{rms}} = 2200\ \mathrm{cm}^{-3}$ and $n_{e,\mathrm{true}} = 2 \times 10^4\ \mathrm{cm}^{-3}$, $\epsilon \sim 0.01$ for W3A. However, since $n_{e,\mathrm{rms}}$ is a lower limit to the average electron density, this value is a lower limit to the filling factor. For most H II regions, the filling factor is found to be in the range of 0.01 to 0.5 (Osterbrock 1989, p. 165). The low filling factor of W3A can be interpreted in terms of extensive clumping in the gas, with most of the ionized matter being concentrated in high-density condensations. This result seems to be appropriate, since the shell-like structure of W3A, with the central low-density cavity (Wynn-Williams 1971) and the high emission measure ionization front observed in radio continuum observations of W3A are obvious signatures of density inhomogeneities.

If the H 171η (∼8.6 GHz) line is pressure broadened, as seems likely (see Adler et al. 1996), the predicted width of the H 168α (∼1.4 GHz) line would be ∼400 km s^{-1}, much larger than the observed value. However, since the H II region is optically thick at 1.4 GHz, the H 168α line from the central hot ionized regions would not be observed. The broad H 168α line detected in the present observations is ∼27 km s^{-1} wide, characteristic of a hot, low-density outer layer of the H II region. There are two possibilities: the outer regions at 9000 K can have an electron density of at most 1100 cm^{-3} if the entire width of the H^+ line is assumed to be attributable to pressure and Doppler broadening. If the widths in these outer regions is only the result of Doppler broadening, the electron density in these outer regions is <1100 cm^{-3}.

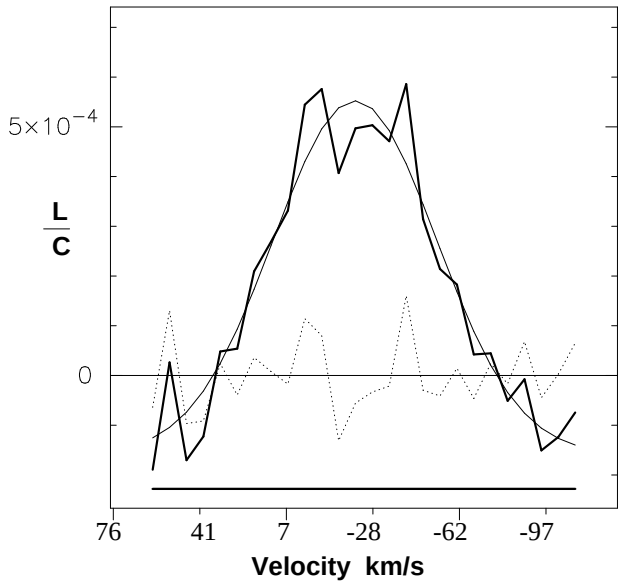

FIG. 8.—The integrated H 171η spectrum observed toward W3A (unpublished data from Uson & Goss). The bold line shows the observed spectrum, the thin solid line is the Gaussian fit, and the dotted line shows the residuals.

5. SUMMARY

We used the VLA to observe the H II region W3A in the 168α recombination lines at 20 cm. In addition to the relatively broad ($\Delta V \sim 30$ km s^{-1}) H^+ line from the H II region, a narrow H^0 line, a C^+ line, and S^+ lines were observed from W3A. The spatial distributions of the these lines were separated using multicomponent Gaussian fits. Analysis of the resulting images has yielded the following results.

1. The distribution of C^+ and H^0 lines over W3A have some similarities, indicating partial overlap. The H^0 lines arise only in the partially ionized medium (PIM), whereas the C^+ lines arise both in the PIM and in the photodissociation regions (PDR). The distribution of carbon lines is quite similar to the molecular gas, as observed in H_2CO with high resolution.

2. An enhancement in the intensities of the H^0 and C^+ lines is observed from the northwest of W3A. The broadest hydrogen lines also arise in this region. Strong [O III] emission, which requires an intense ultraviolet field, has also been observed from this region (Dickel 1983). These data support the suggestion (Roelfsema et al. 1987) that the H II region is breaking out from the molecular cloud.

3. The enhanced C 168α emission near W3A has no counterpart in the lower angular resolution [C II] 158 μm fine-structure line. The dominant contribution to C^+ and to the [C II] 158 μm fine-structure line in W3A appears to be from different components of the ionized gas. This result is

different from that for W3B. Adler et al. (1996) found a strong correlation between C 92α emission and the [C II] 158 μm line (Howe et al. 1991) in W3B, suggesting that the two lines may arise in the same gas. Higher resolution observations of the [C II] 158 μm line are required for a more reliable comparison.

4. The observed width (~ 7 km s^{-1}) of the H^0 line puts a upper limit of ~ 1000 K on the electron temperature of the PIM. If it is assumed that the H^0 and C^+ lines arise in the same gas, the difference in the widths of the lines implies a temperature of 400 K. The observed molecular densities ($\sim 10^5$ cm^{-3}) impose an upper limit on the electron density of 1–60 cm^{-3} in the PDR and 1–80 cm^{-3} in the PIM. Spontaneous emission models for H^0 line are ruled out by the Roger-Dewdney limit on the size of the dissociation region around an O6 star. The observed H^0 line emission is produced by stimulated emission from a background thermal radiation field. Modeling the observed line intensity as arising from stimulated emission, we find that the observed H^0 intensity can arise in a cloud at $T_e = 100$–1000 K and $n_e = 10$–80 cm^{-3}. Stimulated emission in a cloud at $T_e = 100$–1000 K and $n_e = 10$–60 cm^{-3} can explain the observed C^+ line emission. Moreover, spontaneous emission models with $T_e = 100$ and $n_e = 10$–60 cm^{-3} can also explain the observed C^+ line intensity.

5. The H^+ line and the thermal continuum observed near 20 cm arise in the same gas. The temperature of this region from the continuum brightness is calculated to be ~ 8700 K. The true electron density derived from a pressure-broadened H 171η line is $\sim 2 \times 10^4$ cm^{-3}, and the root mean square electron density derived from the measured continuum flux at an optically thin frequency is ~ 2200 cm^{-3}. These values of $n_{e,\mathrm{rms}}$ and $n_{e,\mathrm{true}}$ imply a filling factor of ≥ 0.01 in W3A.

The National Radio Astronomy Observatory is a facility of the National Science Foundation operated under cooperative agreement by Associated Universities, Inc. We thank Paula Benglia for her participation in this project in 1993.

REFERENCES

Adler, D. S., Wood, D. O. S., & Goss, W. M. 1996, ApJ, 471, 871
Anantharamaiah, K. R., Goss, W. M., & Dewdney, P. E. 1990, in Radio Recombination Lines: 25 Years of Investigation, ed M. A. Gordon & R. L. Sorochenko (Dordrecht: Kluwer), 123
Dickel, H. R., Goss, W. M., & Condon, G. R. 1996, ApJ, 460, 716
Dickel, H. R., Harten, R. H., & Gull, T. R. 1983, A&A, 125, 320
Georgelin, Y. M., & Georgelin, Y. P. 1976, A&A, 49, 57
Harris, S., & Wynn-Williams, C. G. 1976, MNRAS, 174, 649
Heiles, C. 1994, ApJ, 436, 720
Howe, J. E., Jaffe, D. T., Genzel, R., & Stacey, G. J. 1991, ApJ, 373, 158
Mezger, P. G., & Henderson, A. P. 1967, ApJ, 147, 471
Onello, J. S., & Phillips, J. A. 1995, ApJ, 448, 727
Onello, J. S., Phillips, J. A., Benaglia, P., Goss, W. M., & Terzian, Y. 1994, ApJ, 426, 249
Osterbrock, D. E. 1989, Astrophysics of Gaseous Nebulae and Active Galactic Nuclei (Berkeley: Univ. Science Books)
Pankonin, V., Walmsley, C. M., Wilson, T. L., & Thomasson, P. 1977, A&A, 57, 341
Payne, H. E., Anantharamaiah, K. R., & Erickson, W. C. 1994, ApJ, 430, 690 (PAE94)
Roelfsema, P. R. 1987, Ph.D thesis, Univ. Groningen
Roelfsema, P. R., & Goss, W. M. 1991, A&AS, 87, 177
Roelfsema, P. R., Goss, W. M., & Wilson, T. L. 1987, A&A, 174, 232
Roger, R. S., & Dewdney, P. E. 1992, ApJ, 385, 536
Salem, M., & Brocklehurst, M. 1979, ApJS, 39, 633
Shaver, P. A. 1969, MNRAS, 142, 273
Subrahmanyan, R., & Goss, W. M. 1996, MNRAS, 281, 239
Tielens, A. G. G. M., & Hollenbach, D. J. 1985, ApJ, 291, 722
van der Hulst, J. M., Terlouw, J. P., Begeman, K., Zwitser, W., & Roelfsema, P. R. 1992, in ASP Conf. Ser. 25, On GIPSY in Astronomical Data Analysis Software and Systems I, ed. D. M. Worall, C. Biemesderfer, & J. Barnes (San Francisco: ASP), 131
van der Werf, P. P., & Goss, W. M. 1990, A&A, 238, 296
van Gorkom, J. H. 1980, Ph.D thesis, Univ. Groningen
Walmsley, C. M., & Watson, W. D. 1982, ApJ, 260, 317
Watson, W. D., Western, L. R., & Christensen, R. B. 1980, ApJ, 240, 956 (WWC80)
Wynn-Williams, C. G. 1971, MNRAS, 151, 397